Compressional and shear-wave velocity structure of the continent-ocean transition zone at the eastern Grand Banks, Newfoundland

Drew R. Eddy,[1] Harm J. A. Van Avendonk,[1] and Donna J. Shillington[2]

Received 25 February 2013; revised 25 April 2013; accepted 25 April 2013.

[1] The seismic structure of the continent-ocean transition (COT) at magma-poor rifted margins can explain geological processes leading to continental breakup. At the Newfoundland-Iberia rift, compressional seismic velocity (V_p) is interpreted with multichannel seismic reflections and drilling results to document continental crustal stretching and thinning, exhumation of the mantle, and incipient seafloor-spreading. However, V_p cannot uniquely constrain COT geology. We present an updated 2-D model for V_p and a new shear-wave velocity model (V_s) for SCREECH Line 2 on the Newfoundland margin using multichannel seismic reflections and coincident ocean-bottom seismometer refraction data. In shallow COT basement we find V_p / V_s ratios average 1.77, which is normally too high for upper continental crust and too low for serpentinized mantle. This observation can be explained by stretching of a mafic middle and/or lower continental crust into the COT. We further support the presence of hydrated mantle peridotites at depth during rifting. **Citation:** Eddy, D. R., H. J. A. Van Avendonk, and D. J. Shillington (2013), Compressional and shear-wave velocity structure of the continent-ocean transition zone at the eastern Grand Banks, Newfoundland, *Geophys. Res. Lett.*, *40*, doi:10.1002/grl.50511.

1. Introduction

[2] Slow rifting at magma-poor margins often occurs without the weakening effects of magmatic diking. Continental crust may be therefore stretched by a large factor ($\beta > 5$), and rocks from the lower continental crust and mantle may be brought to shallow depths via detachment faults [*Whitmarsh et al.*, 2001]. During the final phases of rifting, brittle faulting and hydrothermal circulation can lead to serpentinization of mantle peridotites, weakening the lithospheric mantle [*Manatschal*, 2004; *Reston and McDermott*, 2011]. Before complete breakup of the lithosphere and the onset of normal seafloor-spreading, a ~100 km wide zone of continental mantle may thus be exhumed to the surface in continent-ocean transition zones (COT) [*Whitmarsh et al.*, 2001]. The polarity of lithospheric detachment faults with respect to the locus of breakup often results in asymmetry at conjugate magma-poor margins [*Manatschal*, 2004; *Lavier and Manatschal*, 2006]. In the footwall of a detachment, small amounts of lower crust and, more extensively, uppermost mantle rocks are exhumed to form the COT. At the conjugate rift flank, continental crust of the hanging wall is often highly thinned and stretched above the upper mantle. Strain localization in weakened mantle rocks eventually leads to complete lithospheric breakup and a gradual increase in melt supply from the upwelling asthenosphere [*Lavier and Manatschal*, 2006].

[3] Continental rifting may be accompanied by small amounts of magmatism even if the lithospheric mantle is relatively cold or significantly depleted during rifting [*Müntener and Manatschal*, 2006]. Although rifting of thick continental lithosphere often produces ample magma by decompression melting, only limited amounts of extrusive volcanism may reach the surface if the extension rate is very low [*Lizarralde et al.*, 2004]. Syn-rift melts can therefore be trapped below thick COT lithosphere, so it is possible that not all magmatism is accounted for in an ocean-bottom seismometer (OBS) refraction study of a rifted margin [*Bronner et al.*, 2011]. A better understanding of the melting history of nominally magma-poor margins is important, because even a small amount of melt introduced in the lithosphere during rifting can alter the style of deformation [*Kaczmarek and Müntener*, 2010].

[4] The Newfoundland-Iberia conjugate margins are a prime example of mature magma-poor rift systems [*Tucholke et al.*, 2007]. A large wealth of data from drilling expeditions and marine geophysical studies here document brittle extension of continental crust, exhumation and serpentinization of continental mantle, and a slow onset of seafloor-spreading. The distal Iberian margin is interpreted as almost entirely exhumed continental mantle with a wide zone of compressional seismic velocities (V_p) between 7.0 and 7.5 km/s [*Whitmarsh et al.*, 2001]. This high-velocity zone in the Iberian COT is capped by lower velocities (V_p = 4–5 km/s) interpreted as mantle rock that was pervasively serpentinized after exhumation [*Dean et al.*, 2000]. A similar evolution has been proposed for the conjugate margin in the Newfoundland Basin [*Sibuet et al.*, 2007], although seismic images from the SCREECH project (Studies of Continental Rifting and Extension on the Eastern Canadian Shelf; Figure 1) suggest that crust in the COT is significantly different. Multichannel seismic (MCS) reflections [*Shillington et al.*, 2006] demonstrate that the Newfoundland Basin lacks the faulted allochthonous crustal blocks that have been imaged off the Iberian margin [*Krawczyk et al.*, 1996]. In addition, V_p in the shallow basement of the Newfoundland Basin is often lower than 6.0 km/s [*Lau et al.*, 2006; *Van Avendonk et al.*, 2006], which may indicate unroofed continental crust or exhumed, highly serpentinized mantle peridotites.

[5] Interpretation of the structure and evolution of the COT is complicated by strong seismic reflections from a

Additional supporting information may be found in the online version of this article.

[1]University of Texas Institute for Geophysics, Jackson School of Geosciences, The University of Texas at Austin, Austin, Texas, USA.

[2]Lamont-Doherty Earth Observatory, Columbia University, Palisades, New York, USA.

Corresponding author: D. R. Eddy, University of Texas Institute for Geophysics, Jackson School of Geosciences, The University of Texas at Austin, Austin, TX 78754, USA. (drew.eddy@utexas.edu)

0094-8276/13/10.1002/grl.50511

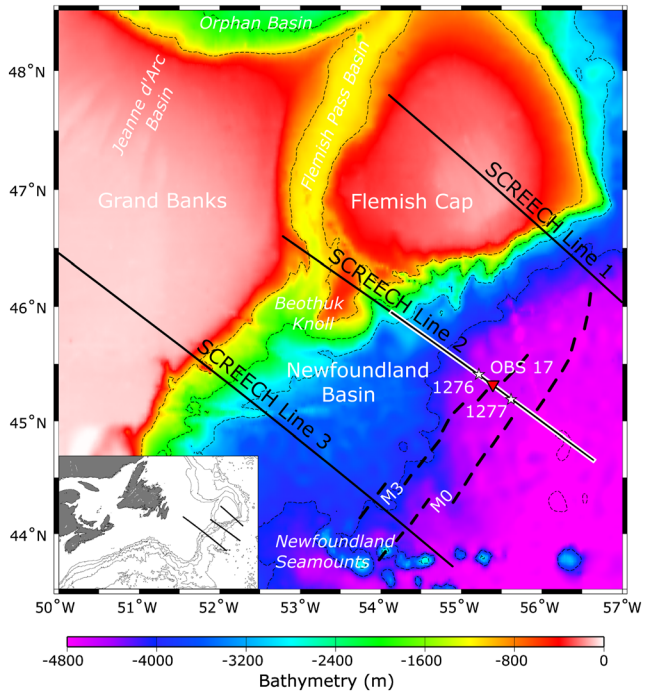

Figure 1. Bathymetric map of the Grand Banks of Newfoundland overlain by 800 m contours, basin features, ODP sites 1276 and 1277 (stars), magnetic anomalies M0 and M3 (dashed lines) [*Srivastava et al.*, 2000], and the location of SCREECH seismic lines (solid lines) and OBS 17 (inverted red triangle). The segment of SCREECH Line 2 analyzed herein is outlined in white. Left lower inset shows Grand Banks in relation to the northeastern seaboard of North America.

package of postrift diabase sills just above the Newfoundland basement at SCREECH Line 2 [*Shillington et al.*, 2008; *Péron-Pinvidic et al.*, 2010]. A large injection of mafic material likely accompanied off-axis volcanism following the complete breakup of the Newfoundland-Iberia lithosphere and production of oceanic crust by the early Albian [*Karner and Shillington*, 2005; *Tucholke et al.*, 2007]. We present an integrated analysis of travel-time constraints from MCS reflection and compressional OBS refraction and reflection data to better characterize the postrift sills and underlying basement on SCREECH Line 2. As a result, we are able to present a new analysis of shear waves that sample the Newfoundland COT basement, and we develop smooth seismic velocity models with regularized tomographic inversions of *P*- and *S*-wave travel times. We use both V_p and V_p / V_s ratio models in our geological interpretations of the rifted margin, assessing our interpretations by plotting seismic velocities with depth at key SCREECH Line 2 intervals. We also use shear-wave data to test simple bulk V_p / V_s models for the flat COT basement.

2. Travel-Time Tomography

[6] The travel times of reflected and refracted phases observed in marine seismic data can be inverted for a layered seismic velocity model with smoothly varying seismic velocities [*Van Avendonk et al.*, 2004, and references therein]. Observation of a series of distinct seismic reflections and refractions in OBS data (Figure 2) provides evidence for layering near the top of crystalline basement that must be included explicitly in the seismic velocity model if we want to correctly model the travel times of later arrivals. We therefore express travel-time residuals for compressional seismic arrivals $\delta T_{p,i}$ as a sum of perturbations δV_p and perturbations in the depth of layer boundaries δz [*Thurber*, 1985; *Van Avendonk et al.*, 2004]. If ray paths calculated in the reference model are good estimates of the true source-receiver paths, this relationship can be approximated with a linearization

$$\delta T_{p,i} \approx \int_{\text{path } i} \frac{-1}{V_p^2}\delta V_p \mathrm{d}s + \sum_{\text{layer } j} \Gamma_{i,j}\delta z_j \qquad (1)$$

[7] The first term of (1) accounts for the contribution to $\delta T_{p,i}$ of seismic velocity perturbations δV_p by integration over the ray path. The coefficient $\Gamma_{i,j}$ represents the partial derivatives of travel-time $\delta T_{p,i}$ with respect to the depth of velocity boundary z_j in the model [*Stork and Clayton*, 1991]. We use (1) to express the model constraints of wide-angle reflections and refractions in the OBS data of SCREECH Line 2 [*Van Avendonk et al.*, 2006], and to incorporate two-way travel times from coincident MCS data [*Shillington et al.*, 2006; *Péron-Pinvidic et al.*, 2010].

[8] To find a smooth seismic velocity model we add spatial first- and second-derivative constraints on the structure of V_p and z to the system of equations (1), and solve them for a model perturbation in a least-squares inversion [*Van Avendonk et al.*, 2004]. This linear inversion step is followed by raytracing in the updated seismic velocity model to calculate new ray paths and travel times. We iterate the raytracing and linearized inversion procedures until we obtain a smooth

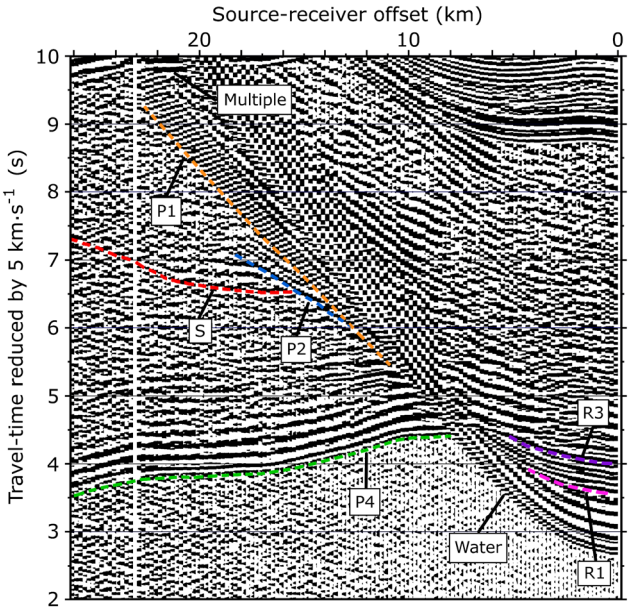

Figure 2. A portion of the receiver gather for OBS 17. See text for descriptions of compressional refractions and reflections (P1–P4, R1–R3). Also labeled are arrivals of the direct wave in water (Water), P4 multiples (Multiple), and a shear-wave refraction (*S*). Additional receiver gathers are available in the Appendix.

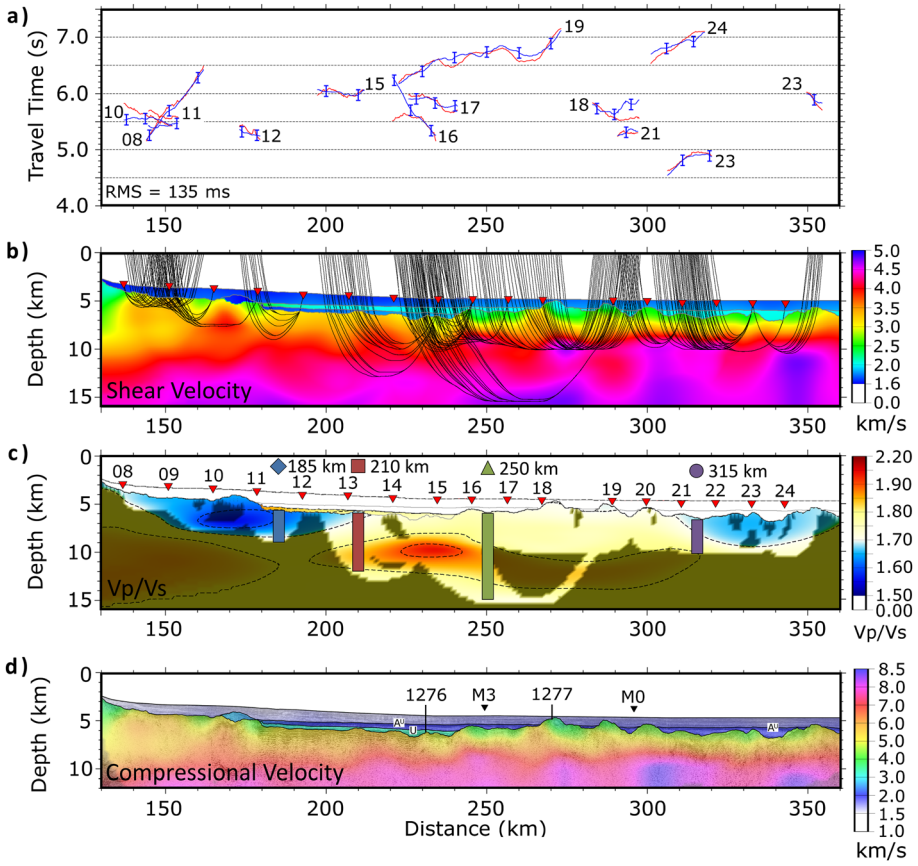

Figure 3. *P*- and *S*-wave seismic velocity structure of SCREECH Line 2. V.E. = ~6:1 for all diagrams. (a) Picked (blue) and calculated (red) *S*-wave travel-time curves. RMS = root-mean-squared misfit. Reduction velocity = 4.0 km/s. *S*-wave uncertainties = 100 ms. (b) Shear velocity structure and calculated *S*-wave paths. (c) V_p / V_s model with depth profiles plotted in Figure 4. Shaded material = unconstrained model space. Red triangles = OBS locations. (d) Compressional velocity structure overlain by coincident MCS data. M3 and M0 = magnetic anomalies. 1276 and 1277 = ODP drilling locations with approximate drill depths. A^U = Horizon A^U. U = U reflection.

seismic velocity model that fits the travel-time data within a specified tolerance level.

[9] Once we have estimated V_p in a profile along SCREECH Line 2, we use a similar procedure to construct a V_s model from shear-wave travel times. However, unlike compressional wave arrivals, shear waves are not consistently observed in OBS records, and their travel times have relatively large uncertainties (100 ms) [*Mjelde et al.*, 2003; *Eccles et al.*, 2009]. We therefore cannot constrain the V_s structure along our profile with the same accuracy as the V_p image. We must also assume that the two models have seismic velocity discontinuities at the same depths z_j. In most studies V_p and V_s appear well correlated [*Brocher*, 2005] such that their ratio $R = V_p / V_s$ may be a more smoothly varying medium property than V_s itself. Accordingly, we express the shear-wave travel-time residual $\delta T_{s,i}$ in R, and we omit terms that assume a dependence on further perturbations of the model layer boundaries z_j

$$\delta T_{s,i} = \int_{\text{path } i} \frac{1}{V_s} \delta R ds \qquad (2)$$

[10] As in the case of the inversion of $\delta T_{p,i}$, we add smoothness constraints for R and solve (2) for this parameter in a least-squares inversion.

3. P-Wave Modeling

[11] We use wide-angle [*Van Avendonk et al.*, 2006] and near-vertical seismic travel-time constraints [*Shillington et al.*, 2006] on the sediments and shallow basement structure along SCREECH Line 2 in a joint inversion of these data with the methodology described in the previous section. The new V_p model, which has detailed information on the sediment and basement interface structure, helps us understand the nature of *P-S* converted waves, which we must interpret before we invert shear-wave travel times for a model of V_p / V_s along SCREECH Line 2.

[12] The choice and geometry of the layers in our new V_p seismic velocity model is guided by MCS imaging of sediments, magmatic sills, and basement along SCREECH Line 2 [*Shillington et al.*, 2006; *Péron-Pinvidic et al.*, 2010] (Figure 3d). *Shillington et al.* [2006] identified two distinct sediment layers above the crystalline basement in their MCS image that are divided by horizon A^U. At larger depth in the COT, *Péron-Pinvidic et al.* [2010] distinguished an interval of anomalously bright reflections topped by the so-called U reflection. This ~1200 m thick sequence lies between the flat basement and overlying sediments, and is interpreted as a package of postrift sills. This interpretation differs from that of *Van Avendonk et al.* [2006, 2009] whose *P*-velocity model for SCREECH Line 2 assumed a

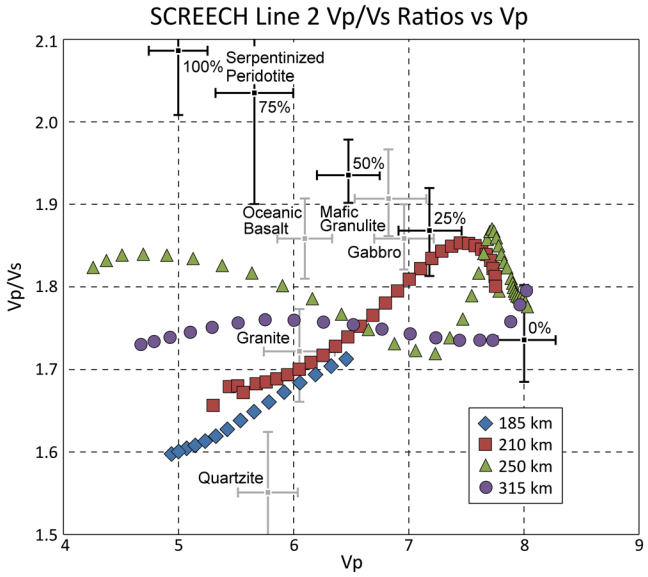

Figure 4. Four depth profiles of V_p / V_s against V_p along SCREECH Line 2. Seismic velocities are plotted every 0.2 km depth for all model space that can be constrained by shear waves in the basement (Figure 3c). Common COT lithologies are also plotted, and values for their seismic velocities can be found in the Appendix.

negligible thickness for the postrift sills in the COT. Basement beneath postrift sills between 180 and 240 km model distance is relatively flat when compared to the highly variable topography of faulted basement at the seaward end of SCREECH Line 2.

[13] In the OBS records of SCREECH Line 2 we interpret three pairs of reflected and refracted phases that appear to be consistent with the layering we describe in the MCS image. We assign four compressional refraction (P1–P4) and three reflection (R1–R3) arrivals in the wide-angle data. As the earliest-arriving phase present in all OBS records, P4 increases in apparent velocity from 5.0–6.0 km/s at 15–20 km offset to 6.0–8.5 km/s at offsets up to 150 km (Figures 2, A2–A5). Local variations in P4 apparent velocity mimic MCS basement relief. Refraction P3 is a straight travel-time branch in *x-t* space and is typically observed at source-receiver offsets of 10–15 km. Apparent velocities for P3 are 2.2–3.2 km/s, with most being slightly higher than 3.0 km/s, on par with the average velocity reported for postrift sill and sediments [*Péron-Pinvidic et al.*, 2010]. The slowest refracted arrivals P2 and P1 intersect the direct water wave with apparent velocities of 1.9–2.5 km/s and 1.7–2.2 km/s, respectively, and their amplitudes diminish at larger offsets. The *x-t* diagrams also show that at short source-receiver offsets the seismic refraction P4 is asymptotic to the wide-angle seismic reflection R3, and both arrivals are observed from each instrument. Limited to instruments above the postrift sills, refraction P3 is asymptotic to reflection R2. Refraction P2 is asymptotic to reflection R1.

[14] We picked 6647 arrival times of *P*-waves from air-gun shots recorded on 17 OBSs between the continental slope and the seaward end of SCREECH Line 2, and 1213 reflection travel times in the coincident MCS data. We assigned uncertainties to these travel times based on pick and data quality. After carrying out the inversion of these data using equation (1), we obtained a new *P*-velocity model that has a low root-mean-square misfit (RMS = 116 ms) and a χ^2 value of 1.0.

4. Shear-Wave and Vp / Vs Modeling

[15] We picked 863 arrival times from shear waves (*S*) turning beneath the basement surface to obtain different constraints on basement structure and composition. Not all of the SCREECH Line 2 instruments have observable *S*-waves (Figure 3a), so the ray coverage in our *S*-wave inversion is more sparse compared to the *P*-wave inversion. *S*-waves have apparent velocities ranging from 3.2 to 4.5 km/s, much lower than phase P4, and often have a variable slope in *x-t* space due to basement depth variations, distinguishing them from compressional refractions with similar (P3) and slightly slower (P1 and P2) velocities.

[16] A challenge with using shear-wave travel times is the fact that the depth of conversion from *P*- to *S*-wave energy in the downgoing raypath is not known. Such conversions may happen at the seafloor or on a deeper boundary with significant impedance contrasts [*Mjelde et al.*, 2003; *Eccles et al.*, 2009]. Based on inspection of the *S*-wave arrivals from SCREECH Line 2, we find that the majority of these observations must represent phases that converted at the top of the basement. We use this assumption to calculate travel-time residuals for the *S*-wave picks and invert the data for a V_p / V_s ratio in the basement, applying equation (2) where we use the V_p model from the tomographic inversion of the previous section. After a few iterations of the raytracing and linearized inversion steps, we obtain a V_p / V_s ratio model (Figure 3c) with a low RMS misfit of 135 ms. It is difficult to quantify the uncertainty in our V_p / V_s model from a statistical standpoint given the paucity of shear-wave data. However, we understand our models to be reasonably well-constrained with average V_p / V_s uncertainties between 0.1 and 0.2 based on comparisons of bulk V_p / V_s models (Figure A1).

[17] To better estimate the lithology of the Newfoundland COT, we plot four depth profiles of V_p against V_p / V_s (Figure 4). Key model distances of 185, 210, 250, and 315 km (Figure 3c) are plotted in an attempt to characterize the most outboard remnant of probable upper continental crust, the region beneath the flat COT basement, the onset of basement with variable topography near ODP 1277, and the seaward end of SCREECH Line 2, respectively. Velocities are plotted every 0.2 km depth for all model space that is constrained by shear waves. SCREECH Line 2 velocities are plotted above established ranges of V_p and V_p / V_s for common COT lithologies (Table A1). For the middle and lower continental crust we plot the felsic rocks quartzite and granite and the mafic rocks gabbro and granulite [*Holbrook et al.*, 1992]. We also plot seismic velocities of basalts found in older oceanic crust [*Hyndman*, 1979; *Brocher*, 2005] and mantle peridotites with 0–100% serpentinization [*Christensen*, 2004].

5. Discussion

[18] Between 130 and 180 km model distance on SCREECH Line 2 (Figure 3), low V_p / V_s ratios (1.57–1.65) are consistent with previous interpretations that this region represents the last portion of the upper continental crust on the Newfoundland margin, including a small package of prerift sediments at ~170 km model distance [*Shillington et al.*, 2006; *Van Avendonk et al.*, 2006]. The uppermost 3.5 km of basement at 185 km model distance (Figure 4, blue diamonds) plots V_p and V_p / V_s consistent with quartzite and

granite [*Holbrook et al*., 1992], supporting the interpretation that continental crust with a predominantly felsic composition typifies this inboard section of the Newfoundland margin.

[19] The most enigmatic aspect of our seismic velocity models is the uppermost 3–5 km of flat COT basement between 180 and 240 km model distance where seismic velocities are relatively homogeneous (V_p = 5.0–6.2 km/s; V_s = 3.0–3.3 km/s) compared to those in the shallow, rough basement immediately seaward. The V_p in the flat COT basement is low enough to be consistent with continental crust [*Holbrook et al*., 1992], as is suggested by *Van Avendonk et al*. [2006]. Other workers contend that the COT in the Newfoundland Basin comprises slow-spreading oceanic crust [*Srivastava et al*., 2000] or exhumed mantle [*Reid*, 1994; *Sibuet et al*., 2007]. Our recovered V_p / V_s ratios alone cannot rule out the possibility proposed by *Srivastava et al*. [2000] that the Newfoundland basement is capped by thin ocean crust, although we note that V_p in the flat COT is lower than what we expect for ocean crust (5.0–7.5 km/s). In this case, weak magnetization in the COT used to support the presence of oceanic crust (e.g., M0 and older; Figure 3d) may be masked by postrift sills above the flat basement [*Péron-Pinvidic et al*., 2010]. Although zones of exhumed continental mantle often have V_p around 7.6 km/s [*Dean et al*., 2000; *Whitmarsh et al*., 2001], mantle peridotites range in V_p from 4.8 to 8.0 km/s depending on the extent of serpentinization [*Christensen*, 2004]. Thus, serpentinized peridotite is a viable explanation for the 5.5 km/s shallow COT basement in the Newfoundland Basin if exhumed mantle rock here is 75% serpentinized. Such a large degree of serpentinization, however, would require *S*-wave velocities as low as 2.75 km/s (V_p / V_s = 2.0). We find that V_p / V_s ratios between 1.67 and 1.77 in the uppermost basement of the COT are too low to primarily represent serpentinized peridotite (Figure 3c). Plots of V_p versus V_p / V_s at 210 km model distance show the top ~2 km of the flat-lying basement approaching velocities of felsic continental crustal rocks (Figure 4, red squares). As V_p increases to >6.5 km/s at depths >5 km beneath the top of basement, the 210 km profile plots more closely to velocities of mafic rocks such as gabbro and/or 10–25% serpentinized mantle peridotite. These results are consistent with interpretations of the uppermost COT basement as unroofed and stretched continental lower crust overlying hydrated mantle peridotites [*Van Avendonk et al*., 2006].

[20] The shallow, rough basement at 250 km model distance between ODP Sites 1276 and 1277 exhibits seismic properties (V_p = 4.0–6.0 km/s; V_p / V_s = 1.72–1.83) that are inconsistent with serpentinized mantle as an average composition (Figure 4, green triangles), although such ultramafic rocks (along with minor amounts of basalt and gabbro) were drilled at Site 1277 [*Robertson*, 2007]. Our model instead plots velocities in the uppermost ~3 km of basement between oceanic basalt and granite, which could indicate the presence of continental rocks far seaward in the COT and/or increasing amounts of volcanics in the shallow basement emplaced during the gradual transition from rifting to seafloor-spreading. Poisson's ratios indicating shallow granodioritic crust (V_p / V_s = 1.78) were similarly found northeast of the Flemish Cap, and a seaward increase in Poisson's ratios (V_p / V_s = 1.86–1.89) near a ridge-like structure were interpreted as a combination of serpentinized mantle and volcanic material [*Gerlings et al*., 2011]. At depths >5 km below the top of SCREECH Line 2 basement, the 250 km depth profile exhibits velocities (V_p >7.7 km/s; V_p / V_s = 1.78–1.88) that match the seismic properties of hydrated mantle rocks and may indicate a decrease in peridotite serpentinization from 25% to 0% with increasing depth.

[21] The most seaward section of SCREECH Line 2 is relatively poorly constrained by the *S*-wave data (Figure 3), and thus the dominant presence of either oceanic crust or serpentinized mantle is equivocal. Furthermore, we cannot rule out gabbroic underplating and melt infiltration at the seaward end SCREECH Line 2 [*Bronner et al*., 2011], which would perhaps be consistent with a gradation from exhumed lithosphere to "incipient" oceanic crust of intermediate composition. The seaward-most V_p versus V_p / V_s plot at 315 km exhibits seismic velocities between granite and oceanic basalt at shallow basement depths, and approaches velocities of minorly serpentinized (0–10%) mantle peridotites at depths of 5 km below basement (Figure 4, purple circles). We caution that plots of seismic properties here may be artifacts of insufficient shear-wave raypath coverage. To image the onset of "true" oceanic crust with normal 6–7 km thickness, additional seismic reflection and refraction data need to be acquired seaward of SCREECH Line 2.

6. Conclusions

[22] Our analysis of V_p / V_s ratios from SCREECH Line 2 supports the hypothesis that highly stretched continental lower crust extends far into the Newfoundland Basin COT. Development of flat basement in the COT was likely shaped by low-angle, landward-dipping detachment faults, although postrift volcanic sills mask the observation of such large-scale faults in MCS data. Shear velocities support the presence of exhumed mantle deep beneath the flat COT basement and around ODP Site 1277, where extensive basement faulting led to partial serpentinization of peridotites that subsequently were infiltrated and overprinted by melt products from the upwelling asthenosphere. Mantle hydration is suggested to decrease with depth. Continued plate divergence between Newfoundland and Iberia led to increasing volcanism that eventually emplaced normal thickness oceanic crust in the Atlantic, but this transition is either not observed at SCREECH Line 2 or is unable to be distinguished from available seismic velocity models.

Appendix

[23] To investigate how well *S*-wave arrivals can constrain V_p / V_s in the COT (and thus distinguish between different possible end-member lithologies), we test how models with three specific V_p / V_s ratios affect *S*-wave travel-time misfits for OBS 15, 17, and 19 in the Newfoundland COT (Figure A1; (a) V_p / V_s = 1.65; (b) V_p / V_s = 1.77; (c) V_p / V_s = 1.87). Blue and red lines represent picked and calculated *S*-wave travel-time curves, respectively. Reduction velocity is 4.0 km/s. To test for the possible presence of felsic continental upper crust, we use a bulk V_p / V_s ratio of 1.65. For more mafic-rich rocks found in oceanic crust or in lower continental crust (either naturally or as exhumed underplated material), we assume V_p / V_s = 1.77 [*Brocher*, 2005]. Alternatively, for mantle peridotites that are 25% serpentinized we assume V_p / V_s = 1.87 [*Christensen*, 2004]. In a few raytracing tests, we keep V_p fixed

Table A1. Compressional and Shear Wave Velocities of Common COT Lithologies[a]

Rock Type	V_p	V_p/V_s	Reference
Quartzite	5.52 ± 0.57	1.55 ± 0.08	*Holbrook et al*. [1992]
Granite	6.07 ± 0.23	1.72 ± 0.05	*Holbrook et al*. [1992]
Oceanic Basalts	6.12 ± 0.21	1.86 ± 0.05	*Hyndman* [1979]; *Brocher* [2005]
Gabbro	6.95 ± 0.22	1.86 ± 0.04	*Holbrook et al*. [1992]
Mafic Granulite	6.86 ± 0.27	1.91 ± 0.05	*Holbrook et al*. [1992]
0% Serpentinized Peridotite	8.02 ± 0.25	1.74 ± 0.06	*Holbrook et al*. [1992]; *Christensen* [2004]
25% Serpentinized Peridotite	7.20 ± 0.25	1.87 ± 0.05	*Christensen* [2004]
50% Serpentinized Peridotite	6.45 ± 0.20	1.94 ± 0.04	*Christensen* [2004]
75% Serpentinized Peridotite	5.70 ± 0.30	2.04 ± 0.14	*Christensen* [2004]
100% Serpentinized Peridotite	5.00 ± 0.25	2.08 ± 0.07	*Christensen* [2004]

[a]Error bars for COT rock types are displayed in Figure 4.

and locally vary the V_p / V_s ratio to determine how it affects the data fit for shear waves that best sample the flat COT basement. The bulk model with V_p / V_s = 1.77 gives the best fit of *S*-wave travel times (RMS = 124 ms). The model with V_p / V_s = 1.87 has a higher misfit (RMS = 183 ms), and a V_p / V_s ratio of 1.65 fits very poorly (RMS = 322 ms). Although not shown in Figure A1, additional testing of bulk V_p / V_s models found that landward of the COT, a low V_p / V_s ratio (1.65) fits the *S*-wave data well, while higher ratios fit poorly. This supports the hypothesis that felsic continental upper crustal rocks characterize the Newfoundland margin here. At the seaward end of SCREECH Line 2, bulk models with V_p / V_s = 1.87 and V_p / V_s = 1.77 produce the lowest misfits (110 and 104 ms, respectively), and the nature of the lithosphere is equivocal given our data.

[24] Appendix figures A2–A5 show receiver gathers for OBS 08, 12, 19, and 23. Refraction and reflection arrivals are described in the text.

[25] **Acknowledgment.** D.R.E. was supported by the Maurice Ewing and J. Lamar Worzel Graduate Student Fellowship from The University of Texas Institute for Geophysics (UTIG contribution #2572). The authors thank Keith Louden and an anonymous reviewer for their comments.

[26] The Editor thanks Keith Louden and an anonymous reviewer for their assistance in evaluating this paper.

References

Brocher, T. M. (2005), Empirical relations between elastic wavespeeds and density in the Earth's crust, *B. Seismol. Soc. Am.*, *95*(6), 2081–2092, doi:10.1785/0120050077.

Bronner, A., D. Sauter, G. Manatschal, G. Péron-Pinvidic, and M. Munschy (2011), Magmatic breakup as an explanation for magnetic anomalies at magma-poor rifted margins, *Nat. Geosci.*, *4*, 549–553, doi:10.1038/ngeo1201.

Christensen, N. I. (2004), Serpentinites, peridotites, and seismology, *Int. Geol. Rev.*, *46*(9), 795–816, doi:10.2747/0020-6814.46.9.795.

Dean, S. M., T. A. Minshull, R. B. Whitmarsh, and K. E. Louden (2000), Deep structure of the ocean-continent transition in the southern Iberia Abyssal Plain from seismic refraction profiles: The IAM-9 transect at 40°20′N, *J. Geophys. Res.*, *105*(B3), 5859–5885, doi:10.1029/1999JB900301.

Eccles, J. D., R. S. White, and P. A. F. Christie (2009), Identification and inversion of converted shear waves: case studies from the European North Atlantic continental margins, *Geophys. J. Int.*, *179*(1), 381–400, doi:10.1111/j.1365-246X.2009.04290.x.

Gerlings, J., K. E. Louden, and H. R. Jackson (2011), Crustal structure of the Flemish Cap Continental Margin (eastern Canada): an analysis of a seismic refraction profile, *Geophys. J. Int.*, *185*(1), 30–48, doi:10.1111/j/1365-246X.2011.04931.x.

Holbrook, W. S., W. D. Mooney, and N. I. Christensen (1992), The seismic velocity structure of the deep continental crust, in *The Lower Continental Crust*, edited by D. M. Fountain, R. Arculus, and R. W. Kay, pp. 1–43, Elsevier, Amsterdam.

Hyndman, R. D. (1979), Poisson's ratio in the oceanic crust – a review, *Tectonophysics*, *59*, 321–333.

Kaczmarek, M. A., and O. Müntener (2010), Juxtaposition of melt impregnation and high-temperature shear zones in the upper mantle; field and petrological constraints from the Lanzo Peridotite (Northern Italy), *J. Petrol.*, *49*, 2187–2220, doi:10.1093/petrology/egn065.

Karner, G. D., and D. J. Shillington (2005), Basalt sills of the U reflector, Newfoundland Basin: a serendipitous dating technique, *Geology*, *33*(12), 985–988, doi:10.1130/G2197.1.

Krawczyk, C. M., T. J. Reston, M.-O. Beslier, and G. Boillot (1996), Evidence for detachment tectonics on the Iberia Abyssal Plain rifted margin, in *Proc. ODP Sci. Results, 147*, edited by R. B. Whitmarsh, et al., pp. 603–615, Ocean Drilling Program, College Station, Texas.

Lau, K. W. H., K. E. Louden, T. Funck, B. E. Tucholke, W. S. Holbrook, J. R. Hopper, and H. C. Larsen (2006), Crustal structure across the Grand Banks - Newfoundland Basin continental margin – I. Results from a seismic refraction profile, *Geophys. J. Int.*, *167*(2), 127–156, doi:10.1111/j.1365-246x.2006.02988.x.

Lavier, L. L., and G. Manatschal (2006), A mechanism to thin the continental lithosphere at magma-poor margins, *Nature*, *440*, 324–328, doi:10.1038/nature04608.

Lizarralde, D., J. B. Gaherty, J. A. Collins, G. Hirth, and S. D. Kim (2004), Spreading-rate dependence of melt extraction at mid-ocean ridges from mantle seismic refraction data, *Nature*, *432*, 744–747, doi:10.1038/nature03140.

Manatschal, G. (2004), New models for evolution of magma-poor rifted margins based on a review of data and concepts from West Iberia and the Alps, *Int. J. Earth Sci.*, *93*(3), 432–466, doi:10.1007/s00531-004-0394-7.

Mjelde, R., H. Shimamura, T. Kanazawa, S. Kodaira, T. Raum, and H. Shiobara (2003), Crustal lineaments, distribution of lower crustal intrusives and structural evolution of the Vøring Margin, NE Atlantic; new insight from wide-angle seismic models, *Tectonophysics*, *369*, 199–218.

Müntener, O., and G. Manatschal (2006), High degrees of melt extraction recoded by spinel harzburgite of the Newfoundland margin: the role of inheritance and consequences for the evolution of the southern North Atlantic, *Earth Planet. Sc. Lett.*, *252*, 437–452, doi:10.1016/j.epsl.2006.10.009.

Péron-Pinvidic, G., D. J. Shillington, and B. Tucholke (2010), Characterization of sills associated with the U reflection on the Newfoundland margin: evidence for widespread early post-rift magmatism on a magma-poor rifted margin, *Geophys. J. Int.*, *182*(1), 113–136, doi:10.1111/j.1365-246X.2010.04635.x.

Reid, I. D. (1994), Crustal structure of a nonvolcanic rifted margin east of Newfoundland, *J. Geophys. Res.*, *99*(B8), 15161–15180.

Reston, T. J., and K. G. McDermott (2011), Successive detachment faults and mantle unroofing at magma-poor rifted margins, *Geology*, *39*(11), 1071–1074, doi:10.1130/G32428.1.

Robertson, A. H. F. (2007), Evidence of continental breakup from the Newfoundland rifted margin (Ocean Drilling Program Leg 210): Lower Cretaceous seafloor formed by exhumation of subcontinental mantle lithosphere, in *Proc. ODP Sci. Results,210*, edited by B. E. Tucholke, et al., pp. 1–69, Ocean Drilling Program, College Station, Texas.

Shillington, D. J., W. S. Holbrook, H. J. A. Van Avendonk, B. E. Tucholke, J. R. Hopper, K. E. Louden, H. C. Larsen, and G. T. Nunes (2006), Evidence for asymmetric nonvolcanic rifting and slow incipient oceanic accretion from seismic reflection data on the Newfoundland margin, *J. Geophys. Res.*, *111*, B09402, doi: 10.1029/2005JB003981.

Shillington, D. J., J. R. Hopper, and W. S. Holbrook (2008), Seismic signal penetration beneath postrift sills on the Newfoundland rifted margin, *Geophysics*, *73*(5), B99–107, doi:10.1190/1.29 72131.

Sibuet, J. -C., S. P. Srivastava, and G. Manatschal (2007), Exhumed mantle-forming transitional crust in the Newfoundland-Iberia rift and associated magnetic anomalies, *J. Geophys. Res.*, *112*, B06105, doi: 10.1029/2005JB003856.

Srivastava, S. P., J. -C. Sibuet, S. Cande, W. R. Roest, and I. D. Reid (2000), Magnetic evidence for slow seafloor spreading during the formation of the Newfoundland and Iberian margins, *Earth Planet. Sc. Lett.*, *182*, 61–76.

Stork, C., and R. W. Clayton (1991), Linear aspects of tomographic velocity analysis, *Geophysics*, *56*(4), 483–495.

Thurber, C. H. (1985), Nonlinear earthquake location: theory and examples, *B. Seismol. Soc Am.*, *75*(3), 779–790.

Tucholke, B. E., D. S. Sawyer, and J. -C. Sibuet (2007), Breakup of the Newfoundland Iberia rift, *Geol. S., Lond., S. P.*, *282*, 9–46, doi:10.1144/SP282.2.

Van Avendonk, H. J. A., D. J. Shillington, W. S. Holbrook, and M. J. Hornbach (2004), Inferring crustal structure in the Aleutian arc from a sparse wide-angle seismic data set, *Geochem. Geophys. Geosyst.*, *5*, Q08008, doi:10.1029/2003GC000664.

Van Avendonk, H. J. A., W. S. Holbrook, G. T. Nunes, D. J. Shillington, B. E. Tucholke, K. E. Louden, H. C. Larsen, and J. R. Hopper (2006), Seismic velocity structure of the rifted margin of the eastern Grand Banks of Newfoundland, Canada, *J. Geophys. Res.*, *111*, B11404, doi: 10.1029/2005JB004156.

Van Avendonk, H. J. A., L. L. Lavier, D. J. Shillington, and G. Manatschal (2009), Extension of continental crust at the margin of the eastern Grand Banks, Newfoundland, *Tectonophysics*, *468*, 131–148, doi:10.1016/j.tecto.2008.05.030.

Whitmarsh, R. B., G. Manatschal, and T. A. Minshull (2001), Evolution of magma-poor continental margins from rifting to seafloor spreading, *Nature*, *413*, 150–153, doi:10.1038/35093085.